

Cover Page



Universiteit Leiden



The handle <http://hdl.handle.net/1887/36998> holds various files of this Leiden University dissertation.

**Author:** Dunnen, Angela den

**Title:** Surface-structure dependencies in catalytic reactions

**Issue Date:** 2015-12-09

## Chapter 3

# Reaction dynamics of initial O<sub>2</sub> sticking on Pd(100)

### Abstract

We have determined the initial sticking probability of O<sub>2</sub> on Pd(100) using the King and Wells method for various kinetic energies, surface temperatures, and incident angles. The data suggest two different mechanisms to sticking and dissociation. Dissociation proceeds mostly through a direct process with indirect dissociation contributing only at low kinetic energies. We suggest a dynamical precursor state to account for the indirect dissociation channel, while steering causes the high absolute reactivity. A comparison of our results to those previously obtained for Pd(111) and Pd(110) highlights how similar results for different surfaces are interpreted to suggest widely varying dynamics.

---

This chapter is based on: A. den Dunnen, S. Wiegman, L. Jacobse, and L.B.F. Juurlink, *J. Chem. Phys.*, 2015, **142**, 214708.

## 3.1 Introduction

Dissociative adsorption of  $O_2$  on metal surfaces is a poorly understood but crucial elementary reaction step to many heterogeneously catalyzed oxidation reactions. Various recent reviews discuss the current level of understanding for prototypical metals, e.g. Al, Pt, Cu, Ag, and Pd<sup>15–17</sup>. Complications in theoretical approaches to accurately describe  $O_2$  dissociation dynamics arise from the high reaction energy that needs to be dissipated into electron-hole (e-h) pairs and/or phonons, and a quenching of the triplet spin state upon dissociation<sup>15</sup>.

$O_2$  dissociation on Pt(111) is one of few systems studied experimentally and theoretically in great detail<sup>18–23</sup>. The reaction has been shown to occur solely via an indirect mechanism<sup>19,21,24</sup>. Stable, molecularly bound chemisorbed states labeled as superoxide ( $O_2^-$ ) and peroxide ( $O_2^{2-}$ ) were identified spectroscopically as the only species on the surface, even at high impact energies<sup>19</sup>. The dissociation of such systems may then be treated by a kinetic model assuming equilibrated states<sup>25</sup>. Figure 3.1 displays a 1-dimensional (1-D) potential for interaction of an  $O_2$  molecule with a surface, containing both a physisorbed and chemisorbed well, as originally proposed for  $O_2/Ag$ <sup>25</sup>, but here modified to have a lower barrier to dissociation than to desorption<sup>26</sup>. In the absence of a significant influence of a physisorbed state, an experimentally determined temperature dependence to dissociation on Pt(111) was used to extract the difference between the desorption energy and the barrier to dissociation from the molecular state ( $\Delta E_{act}$ )<sup>24,26</sup>. The adsorption energy of the molecular and atomic states ( $\Delta E_{O_2,chem}$  and  $\Delta E_{2O_{ads}}$ ) may be derived from e.g. single crystal adsorption calorimetry (SCAC) and temperature programmed desorption (TPD). Such data yield references for theoretical studies that map the potential energy surface (PES) for the same system.

The effect of molecular precursor states on the dissociation dynamics as probed by molecular beam techniques is dependent on their location and depth within the full PES<sup>27,28</sup>. Obviously, both parameters change with the identity of the metal and surface structure. Moving from Pt to Pd, the reaction energy for dissociation of  $O_2$  increases<sup>29</sup>. As the atomic well depth increases, the barrier between the atomic and molecular state is lowered unless the molecular state is stabilized by the same amount. Motion of the molecular state along the reaction coordinate also affects the barrier. Hence, in moving from Pt to Pd, the relevance of the molecular precursor state may alter or remain the same. For Pd(111), spectroscopic identification of

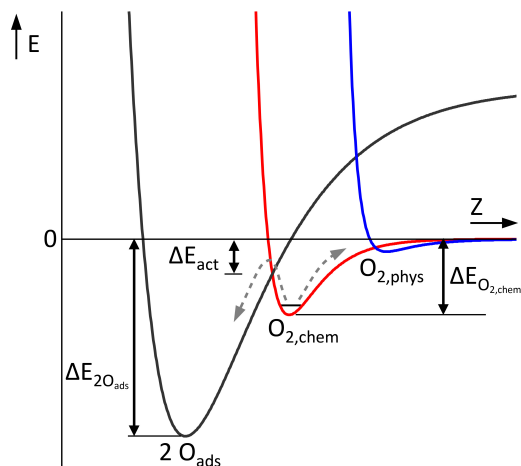


**Figure 3.1:** Schematic 1-D representation of a potential energy surface for  $O_2$  dissociation on a metal surface. The blue line indicates the  $O_2$  physisorption well ( $O_{2,phys}$ ), the red line the  $O_2$  chemisorption well ( $O_{2,chem}$ ), and the black line the dissociated oxygen well ( $O_{ads}$ ).

$O_{2,chem}$  and molecular beam studies indicate that dissociation occurs via an equilibrated molecular  $O_2$  state similar to Pt(111)<sup>30</sup>. A theoretical study using *ab initio* local spin density calculations agrees<sup>29</sup>.

For Pd(100), an electron energy loss spectroscopy (EELS) study finds that on the bare surface  $O_2$  dissociates even at 10 K<sup>31</sup>. At higher exposures, but prior to completion of the  $p(2 \times 2)$  surface structure at 0.25 monolayer (ML) coverage<sup>31–38</sup> molecularly adsorbed oxygen is observed<sup>31,33</sup>. This may be taken to imply that there is no significant barrier between an adsorbed molecular and dissociated state for oxygen on the bare surface. The appearance of a molecular state on O/Pd(100) may result from a significant change in its binding energy due to the presence of atomic oxygen in a next-nearest neighbor (NNN) site on the surface. It could also reflect a metastable molecular state on the bare surface that is not significantly changed, but cannot dissociate as a result of site blocking at the nearest neighbor (NN) site.

Various cuts through high dimensionality PESs for  $O_2$ /Pd(100) were recently published independently by two research groups<sup>39–41</sup>. Both PESs show a deep molecular chemisorption well located at the fourfold hollow site with the internuclear  $O_2$  axis pointing toward bridge sites. The molecular state has a binding energy of

$\sim 1.5$  eV per  $O_2$ . The deep molecular well is located at a short distance from the surface and stretched along the O-O internuclear distance axis<sup>40,41</sup>. Hence, the barrier to dissociation is purely located in the exit channel. Barrier heights of 120<sup>39</sup> or  $\sim 200$  meV<sup>41</sup> separate the molecular state from the dissociated state. The dissociation occurs by motion of both O atoms across opposite bridge sites. Meyer and Reuter find the dissociation to release 2.6 eV per  $O_2$  in total, very little of which is coupled non-adiabatically to e-h pair excitation<sup>40</sup>. Dynamical calculations indicate that most of the dissipated energy is quickly absorbed by a heat bath, while the O atoms retained a significant amount of kinetic energy after dissociation<sup>42</sup>. Coverage dependent calculations of the barrier to dissociation from the molecular state by Liu and Evans indicate that increased occupancy of NNN sites of the fourfold hollow where  $O_2$  adsorbs both weakens the adsorption energy of the molecular state and increases the barrier to dissociation<sup>39</sup>. Other cuts of both PESs with the  $O_2$  internuclear axis (nearly) parallel to the surface suggest the presence of modestly-activated dissociative adsorption pathways at bridge and top sites<sup>39,41</sup>. At other locations and for other angles between the surface and the molecular axis, the PES becomes strongly repulsive. The cuts through the potential therefor imply a high level of corrugation. Hence, this PES exhibits interesting characteristics that may be probed experimentally.

Here, we present our results from an investigation into the dissociation dynamics of  $O_2$  on Pd(100) using supersonic molecular beam techniques. General trends in sticking probability ( $S_0$ ) observed as function of incident kinetic energy ( $E_i$ ), surface temperature ( $T_s$ ), and incident angle ( $\theta$ ) dependencies are discussed in terms of possible sticking and dissociation mechanisms. Our results are also compared to those for other low-Miller-index Pd surfaces. We suggest implications for the aforementioned and future theoretical studies of  $O_2$ /Pd(100).

## 3.2 Experimental

### 3.2.1 The apparatus

Experiments were performed using an ultra-high vacuum (UHV) apparatus (base pressure  $< 1 \cdot 10^{-10}$  mbar) equipped with a double differentially pumped supersonic molecular beam and a single differentially pumped effusive beam. These beams intersect at the surface of a sample that is suspended from a liquid nitrogen cooled

cryostat on an  $x, y, z, \theta$  manipulator. The UHV chamber also contains a fixed quadrupole mass spectrometer (Pfeiffer, QMA 200) for TPD, residual gas analysis (RGA), and King and Wells (KW) measurements, a quadrupole mass spectrometer (UTI 100C) which can be moved along the molecular beam axis for time-of-flight (TOF) measurements, a LEED/Auger (RVL 2000/8/R) apparatus, a sputter gun, and various leak valves.

Supersonic molecular beams were created by continuous expansion of gas mixtures at 0.5-4.7 bar through a tungsten nozzle with a circular 45  $\mu\text{m}$  diameter orifice at room temperature. A beam was shaped by a set of three skimmers separating the source, two differential, and one UHV chamber. Flags in the second differential and UHV chamber and a chopper wheel in the first differential chamber modulate the beam. The incident kinetic energy of the molecular beam was controlled by seeding or antiseeding with helium (Linde, 6.0) or argon (Air Products, 5.7). The (spread in) kinetic energy of the  $\text{O}_2$  in our beams was determined by TOF. The (initial) sticking probabilities were determined using the King and Wells technique<sup>8</sup>. Exposure of the crystal to the beam is continued until the exposed surface area has reached a maximum coverage. Coverage dependent sticking and our subsequent TPD experiments are discussed in chapter 4.

### 3.2.2 The Pd(100) crystal

Initially, we employed a Pd(100) single crystal that was previously used in high-pressure CO oxidation studies<sup>43,44</sup>. The crystal was extensively cleaned by repeated cycles of  $\text{Ar}^+$  bombardment (Messer, 5.0; 15  $\mu\text{A}$ , 5 min.), annealing at a surface temperature of 900 K in an oxygen atmosphere (Messer, 5.0;  $3.5 \cdot 10^{-8}$  mbar, 3 min.), and 3 minutes of vacuum annealing at a surface temperature of 1200 K. The surface cleanliness was confirmed by comparison of known TPD spectra for  $\text{H}_2$  and  $\text{O}_2$ . We did not observe any significant CO formation in temperature programmed reaction when titrating the cleaned surface with  $\text{O}_2$ . Long-range surface order was confirmed by low energy electron diffraction (LEED). In between subsequent KW measurements, the crystal was vacuum annealed for 3 minutes at a temperature of 1200 K. Consistency of results was checked by regularly repeating an experiment under identical conditions. After obtaining an initial set of data for  $S_0(E_i)$ , an unexpected weak dependence on incident energy caused concerns regarding the quality of the crystal. Hence, we repeated all experiments on a newly-purchased Pd

single crystal. This second crystal was cut and polished to expose the (100) plane to  $< 0.1^\circ$  accuracy (Surface Preparation Laboratory, Zaandam, The Netherlands). After an initial extensive cleaning procedure, no significant differences between the results from our two crystals were observed when using the same procedures for cleaning and determining  $S_0$ . The measurements on the new crystal were extended to include surface temperature and angle dependencies. The kinetic energy and surface temperature dependencies were also determined a second time with an interval of almost two years. Minor variations ( $< 5\text{-}10\%$  depending on kinetic energy) in averaged absolute sticking probability for multiple measurements were found between these two data sets.

### 3.2.3 $S_0$ determination

Reactive molecules may cause difficulties in obtaining correct values for  $S_0$  as the walls and filaments in the UHV chamber can act as pumps in parallel to the surface of interest<sup>45</sup>. Figure 3.2 illustrates that our  $S_0$  measurements suffer somewhat from a transient observed in the first second after the cleaned and very reactive Pd(100) is exposed to a supersonic molecular beam containing  $O_2$ . The insets of figure 3.2 show the actual  $O_2$  KW traces for (a)  $E_i = 0.42$  eV and (b) 0.058 eV at a surface temperature of 100 K and normal incidence. They also present two extremes in the variation of KW trace shapes. The KW traces are background corrected, inverted, and scaled between 0 and 1 to yield the time-dependent sticking probability curves. The latter are shown, expanded between 0 and 5 seconds, in the main figure.

The transient behavior in the first second may result from various convolutions. The time required to fully ‘open’ the beam by removal of the main chamber flag is only  $\sim 3$  ms. The transient is therefore most likely an artifact resulting from our system’s vacuum time constant for  $O_2$  ( $\sim 55$  ms) and possibly a change in the effective pumping speed when allowing the beam to impinge upon the highly reactive Pd(100) surface. For high kinetic energies and/or high surface temperatures, the transient leads to an underestimation of  $S_0$  if we were to take the highest point on the sticking over time ( $S(\text{time})$ ) trace. We have attempted to eliminate the transient by reducing the  $O_2$  flux. However, reducing the beam to a maximum of 8%  $O_2$ , retracting the nozzle from the first skimmer, and chopping the beam at  $\sim 250$  Hz using a chopper wheel with a 16% duty cycle did not remove it. Hence, we obtain  $S_0$  by extrapolating a linear section of  $S(\text{time})$  to the exact time where the second flag

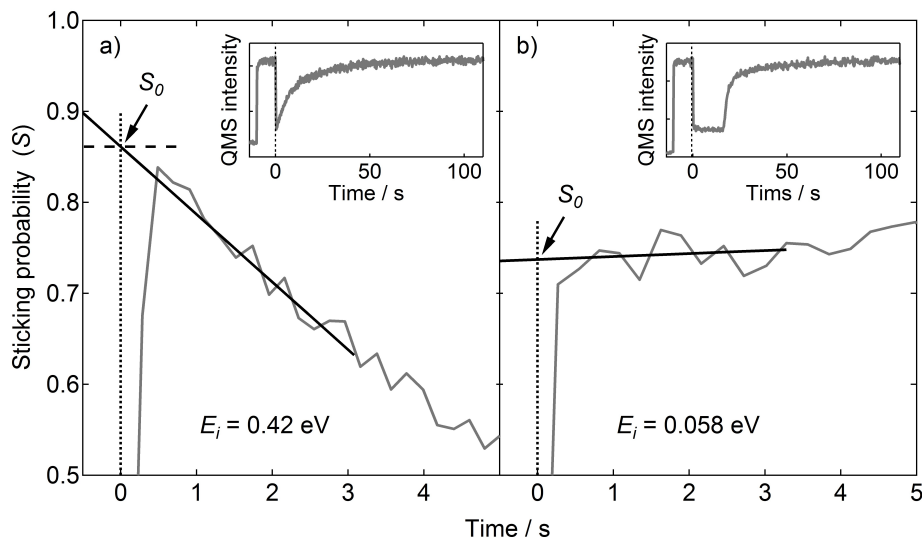


**Figure 3.2:** Time-dependent sticking traces for  $\text{O}_2$  on Pd(100) at normal incidence and  $T_s = 100$  K for (a)  $E_i = 0.42$  eV and (b)  $0.058$  eV. The reported values for  $S_0$  are determined by extrapolation to the exact time of opening of the second flag. Original KW traces are shown as insets.

opens. Figure 3.2 illustrates this procedure. For high kinetic energies and surface temperatures it increases  $S_0$  on the order of 0.05 relative to the highest point on the  $S_0$  trace, whereas it does not affect the value obtained for low kinetic energies and low surface temperatures. Values for  $S_0$  reported here are averaged values of multiple measurements using the second Pd(100) crystal described above. The maximum standard deviation in  $S_0$  of multiple measurements within a single data set was found to be 0.026. For the energy dependence, measurements were performed 2 to 6 times and repeated regularly during a single or multiple days. The spread in incident energy for a single beam is typically less than 20% of the incident energy. For one single beam of 0.32 eV, a larger energy spread of almost 50% was found.

The sticking probability is very high, but does not reach unity even at high incident energy. We have verified that this is not a consequence of contamination picked up by the crystal in between cleaning and starting the KW experiment. Pre-dosing  $\text{H}_2$ , i.e. the dominant residual gas, for 60 seconds at  $1 \cdot 10^{-9}$  mbar causes a decrease in  $S_0$  of 0.15 for the surface at 100 K. It does not influence the  $S_0$  for the

400 K surface. Considering the  $H_2$  partial pressure and typical time lag, we underestimate  $S_0$  only for surface temperatures below 400 K and at most by a couple of percent.

### 3.3 Results and discussion

Figure 3.3 visualizes the trends of  $S_0(E_i, T_s, \theta)$  for  $O_2$  on Pd(100). The blue and red lines indicate a surface temperature of 100 K and 400 K, respectively. The actual data are shown in figures 3.4, 3.5, and 3.6. To create figure 3.3, we have used a polynomial fit to reflect the energy dependence. We have used all data from two data sets gathered over a two year time span for the new crystal in the fitting procedure. For the angle dependence, we have used a cosine fit. Here only one data set was available. The additional light blue curve in the 0.42 eV plane reflects the expected angle dependence if normal energy scaling would be observed using the data for  $T_s = 100$  K to fix  $S_0$  at normal incidence.

We summarize characteristics of the general trends observed in figure 3.3. First, the  $S_0(E_i)$  dependence (detailed in figure 3.4) shows a slight initial decrease with increasing incident energy. Thereafter, a gradual increase is observed that seems limited to a maximum value near 0.9. Second,  $S_0$  is nearly independent of surface temperature over the entire energy range. The minor dependence appearing in figure 3.3 is actually caused by site-blocking from residual  $H_2$  dissociation occurring while the crystal cools to 100 K. We have verified experimentally that  $H_2$  pre-dosed on purpose at 100 K lowers  $S_0$ . The second data set probing temperature dependence is shown in figure 3.5, was taken after our crystal's cooling rate had been improved significantly. It shows no significant  $T_s$  dependence over the entire energy range from 100 K to 400 K and from 0.056 to 0.38 eV. Third, we observe two opposite angle dependencies (also shown in figure 3.6) at low and high incident energies. At low incident energy and  $T_s = 400$  K, there is no angle dependence, while at 100 K,  $S_0$  even slightly increases with angle. At higher kinetic energies, the angle dependence reverses and weakly resembles normal energy scaling. Note that our crystal rotates along an axis  $27^\circ$  away from [011] in the direction of  $[0\bar{1}1]$ .

These trends are explained by two parallel dissociation mechanisms, whose contribution depend on incident energy. At low  $E_i$ , an initial decline in  $S_0$  points toward an indirect mechanism or steering. The subsequent increase in  $S_0$  with

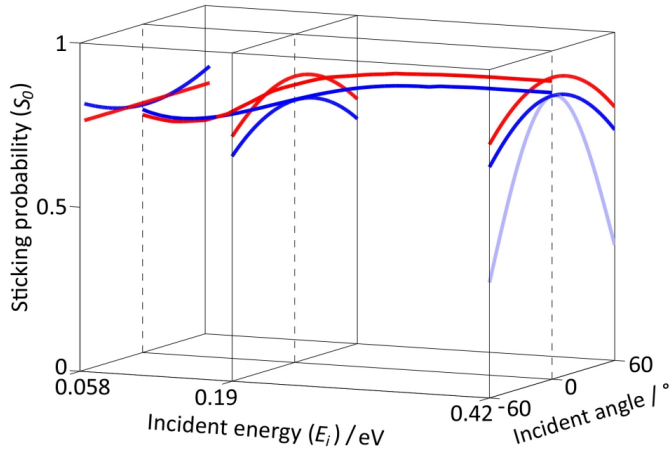


**Figure 3.3:** A 3-dimensional overview of  $O_2$   $S_0$  on Pd(100) as a function of  $E_i$  (fitted with polynomial function) and incident angle (fitted with cosine function) at  $T_s = 400$  K (red lines) and 100 K (blue lines). The light blue line in the 0.42 eV plane shows the normal energy scaling for  $T_s = 100$  K.

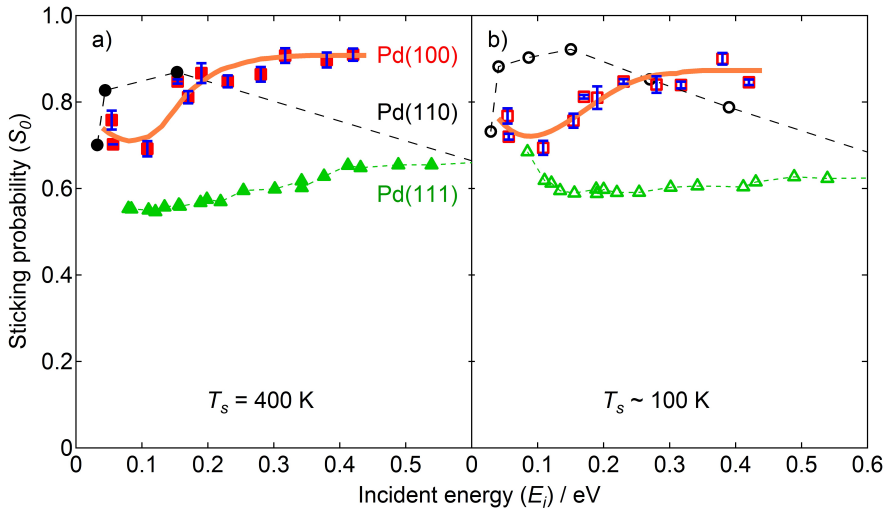


**Figure 3.4:**  $S_0$  of  $O_2$  on Pd(100) (red squares with blue error bars (standard deviation in y-direction)), Pd(111) (green triangles)<sup>30</sup>, and Pd(110) (black circles, (b) at  $T_s = 102$  K)<sup>46</sup> as a function of  $E_i$  at (a)  $T_s = 400$  K and (b) 100 K. Lines are a guide to the eye. They include data for Pd(110) and Pd(111) that fall outside the energy range shown here.

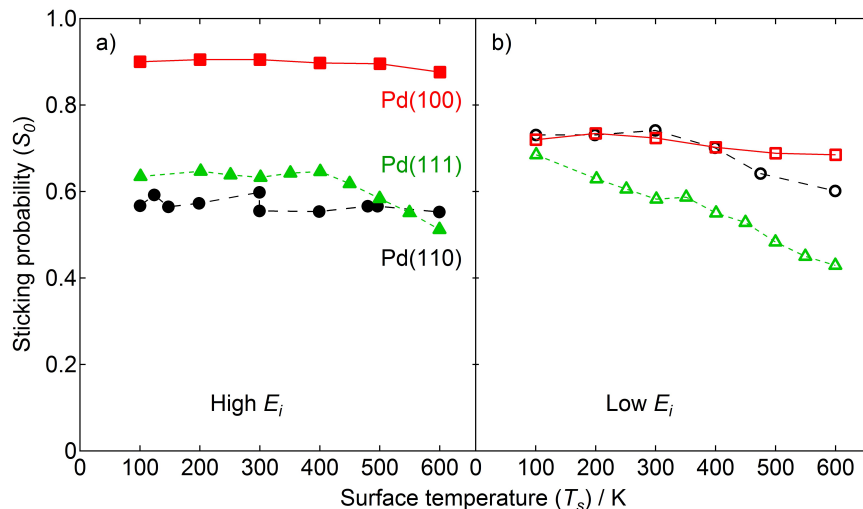


**Figure 3.5:**  $S_0$  as a function of  $T_s$  at (a) high and (b) low incident energy for Pd(100) ( $E_i = 0.38$  eV and 0.056 eV, red squares), Pd(111) ( $E_i = 0.69$  eV and 0.083 eV, green triangles)<sup>30</sup>, and Pd(110) ( $E_i = 0.84$  eV and 0.032 eV, black circles)<sup>46</sup>.

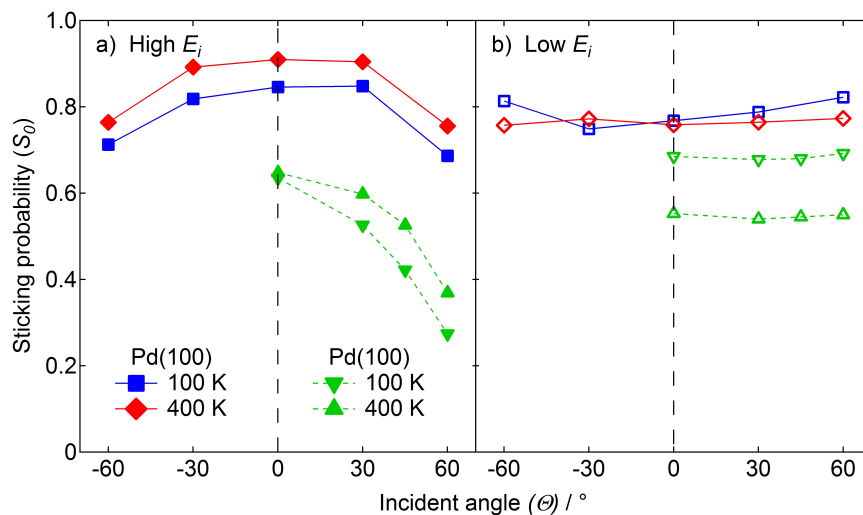


**Figure 3.6:**  $S_0$  of  $O_2$  on Pd(100) (blue squares at  $T_s = 100$  K, red diamonds at 400 K at 0.058 eV and 0.42 eV) and Pd(111) (green point down triangles at  $T_s = 100$  K and point up triangles at 400 K at 0.084 eV and 0.69 eV)<sup>30</sup> as a function of incident angle for (a) high and (b) low  $E_i$ .

$E_i$  suggests an increasing dominance of a direct mechanism that benefits from momentum normal to the surface. We first focus on the indirect mechanism.

An indirect mechanism at low  $E_i$  is often ascribed to sticking and dissociation via an equilibrated or dynamic molecular precursor. However, steering may also cause a decline in reactivity<sup>47–49</sup>. The absence of a temperature dependence in our data argues against an equilibrated precursor. On the other hand, a dynamical precursor mechanism, as suggested to dominate H<sub>2</sub> dissociation on stepped Pt surfaces at low kinetic energies<sup>50,51</sup>, explains our surface temperature independence. The (near) absence of an angle dependence at low incident energies also agrees with a dynamic precursor mechanism. For H<sub>2</sub> on stepped Pt surfaces, a small linear angle dependence was attributed to the asymmetry of the stepped surface structure<sup>50,52</sup>. Steering, as argued to strongly influence H<sub>2</sub> dissociation on Pd(100)<sup>49,53</sup> and O<sub>2</sub> dissociation on Pt(111)<sup>22,23</sup>, would also not show a surface temperature dependence. However, molecular dynamics simulations for O<sub>2</sub> on Pt(111) show an angle dependence to sticking at all energies while sticking is effectuated by steering. This seems at odds with our observations. However, O<sub>2</sub> sticking on Pt(111) proceeds via an equilibrated molecular state, which is likely positioned elsewhere along the reaction coordinate compared to Pd(100). Hence, we do not consider a different angle dependence a reason to exclude steering as a potential cause for the high reactivity and angle independence. The high level of corrugation actually makes steering likely, particularly at low  $E_i$ .

The observed coverage independent sticking probability at 100 K and low  $E_i$ , as shown in the inset of figure 3.2b, invites an explanation in terms of sticking via an extrinsic precursor state<sup>54–56</sup>. Again, our temperature independence at low energy and the aforementioned EELS results argue against a stable molecular state in the zero-coverage limit. The depth of the O<sub>2,chem</sub> well, as found in the theoretical studies, also makes it unlikely that a physisorbed state is influential to the sticking and dissociation dynamics. In this regard, it is noteworthy that O<sub>2</sub> dissociation on (100) surfaces is generally believed to require two additional empty fourfold hollow sites (8-site model)<sup>57,58</sup>. For Pd(100), these additional empty sites are on opposite sides across the bridges<sup>42</sup>. If either one is occupied or a NNN site is occupied, the exit channel is hampered or cannot be entered entirely. However, the molecule may equilibrate in the molecular state. In the coverage dependence study of the stability of the molecular state by Liu and Evans<sup>39</sup>, O<sub>2</sub> is still bound by 0.9 eV when all NNN sites are occupied. The barrier to dissociation has increased from 0.12 eV to 0.4 eV,

while the desorption energy is dropped from 1.5 to 1.3 eV. Hence, we expect that the coverage independence observed in our experiments for low  $T_s$  and  $E_i$  follows from reducing the ease with which the exit channel to dissociation is reached with increasing coverage, effectively making the metastable molecular state more stable. A drop in sticking from dissociation via a (steered) dynamic precursor state is counterbalanced by scattering and sticking in the molecular state. This ultimately leads to a considerably higher total O/Pd coverage when performing the experiment at 100 K than under conditions that only lead to the  $p(2 \times 2)$  structure with the 0.25 ML coverage or higher coverages reported for prolonged exposures<sup>32,34,36</sup>. Our TPD results are fully in line with this interpretation. TPD spectra even provide evidence of a molecular state that is occupied at high coverage and low surface temperature (see chapter 4). Summarizing, we interpret our data at low  $E_i$  in the zero-coverage limit to suggest a gradual, near barrier-free transition of  $O_{2,\text{phys}}$ ,  $O_{2,\text{chem}}$ , and  $O_{\text{ads}}$  sites for  $O_2$  on Pd(100). With increased coverage, trapping in the molecular state becomes possible.

When increasing  $E_i$ , the weak downward trend in sticking quickly reverses. Such behavior can be explained by an increasingly dominant direct mechanism<sup>59</sup>. Translational energy may help overcome activation barriers along reaction paths other than the minimum energy path. It may also allow for a larger range of trajectories to reach a state from which returning into the gas phase is impossible. A second option is an activated molecular chemisorption pathway. This molecularly chemisorbed state may be a precursor to dissociation. Our observations of a decrease in reactivity with increasing angle, an independence on surface temperature, the previously observed absence of a stable  $O_{2,\text{chem}}$  state in EELS studies<sup>31</sup>, and the suggested presence of weakly activated dissociative pathways on other surface sites than the fourfold hollow in density functional theory (DFT) calculations<sup>39,41</sup> all favor the direct dissociation mechanism. The angle dependence observed for higher kinetic energies may indicate that slightly activated pathways have a barrier positioned toward the entrance channel. They become accessible at increased energy.

We continue with a comparison of the dissociation dynamics for Pd(100) with Pd(111) and Pd(110). The available experimental data of  $S_0(E_i, T_s, \Theta)$  for Pd(110)<sup>46</sup> and Pd(111)<sup>30</sup> are reproduced from the literature in figures 3.4, 3.5, and 3.6.

The energy dependence of  $O_2$  sticking on Pd(111)<sup>30</sup> shows strong similarities with Pd(100). First, it shows a drop, then a slow rise. The angular dependence also

compares well to our results. However, in contrast to Pd(100),  $S_0$  for Pd(111) shows a strong dependence on surface temperature. At low energy,  $S_0$  decreases fast over the entire temperature range. At high energy, it is independent of  $T_s$  up to 400 K beyond which  $S_0$  decreases. Here, the drop can not be ascribed to a competing onset of associative desorption<sup>60</sup>. The observations for Pd(111) were explained by sequential physisorbed and chemisorbed precursor states for low  $E_i$ , while at high  $E_i$  O<sub>2</sub> directly chemisorbs as a molecule. Direct dissociation was not observed for energies up to 0.69 eV. Theoretical calculations for this system<sup>29</sup> support stable molecular intermediates for this surface. Equilibrated molecular O<sub>2</sub> states were also identified for Pd(111) by EELS<sup>61</sup>.

For Pd(110)<sup>46</sup> the temperature dependencies are similar to Pd(100), but an opposite trend in the kinetic energy dependence is observed. Here,  $S_0$  increases up to 0.16 eV. Although the highest energy data lie outside our axis range, the dashed lines connecting the data show that at higher energies  $S_0$  strongly decreases. These trends were ascribed to a very attractive molecularly chemisorbed precursor state leading to dissociation at low incident energy and a direct activated adsorption channel opening at higher energies. The maximum in  $S_0$  was described as resulting from the sum of these two parallel processes with inverse dependencies on kinetic energy as used in the explanations for trends observed on Pd(100) and Pd(111).

### 3.4 Summary

For all low-Miller-index Pd surfaces, molecular chemisorbed states are invoked to influence the dynamics of O<sub>2</sub> dissociation. On Pd(111) and Pd(110), the chemisorbed state is considered a stable intermediate. It is directly or indirectly accessible from the gas phase, depending on kinetic energy. The location and depth of its potential well warrant it to be a separate state with barriers between the physisorbed and atomic states. For Pd(100), we find no reason to invoke a stable molecular state in our experiments probing reactivity in the zero coverage limit. Our findings support previous suggestions by other experiments and theory. This implies that the molecular state's location is positioned far along the reaction coordinate and/or is of significant depth when compared to the atomic state. Either argument leads to a loss of a significant barrier between the molecular and atomic states. This implication is reflected in the cuts of the PES and the limited dynamics studies published

to date for  $O_2$ /Pd(100). A deep molecular chemisorbed state would also lead to a lesser importance of a physisorbed state. Steering may be an important ingredient to explain the high reactivity at all kinetic energies.

Although virtually invisible to experiments, the molecular chemisorbed state for  $O_2$  /Pd(100) is of high relevance for two reasons. For the attractive part, it presents an easy path with little corrugation connecting the physisorbed to atomic states. The repulsive part of the molecular state is crucial in the required energy-loss mechanism during the encounter of  $O_2$  with the surface. It is the first encounter of the impinging molecule with the repulsive wall of the molecular state that fully determines whether the molecule loses enough energy to trap it in a dynamic precursor state. Our explanation of the nearly independence of sticking with coverage from counterbalancing reduction of dissociative sticking by scattering into a stabilized molecular state from exit channel blocking, requires that energy transfer must be nearly independent of the local environment. The very slight increase in  $S_0$  with coverage suggests that energy transfer is even better when a molecule happens to impinge on or near a fourfold hollow occupied by  $O_2$  or O. The slight positive angle dependence at the lowest total energies may indicate that the chance to be steered into the metastable molecular state improves when the molecule moves more slowly along the surface normal. The parallel momentum and associated energy for off-normal incidence are very small compared to the energy gain when the molecule enters into the molecular well. It is therefore irrelevant and disappears by the efficient excitation of the in-plane surface-phonon modes when the molecule starts moving up the repulsive wall of the  $O_2$  molecular state<sup>42</sup>. The large loss of energy and excitation of phonon modes upon that first encounter with the surface can be seen in the energy redistribution for a reactive encounter depicted for a reactive trajectory by Meyer and Reuter<sup>42</sup>. Figure 3.7 schematically illustrates our suggestion.

### 3.5 Conclusion

For Pd(100), we suggest that dissociative adsorption on the bare surface at the lowest incident energy occurs via a dynamic precursor. The efficiency of entering into the molecular state is likely positively affected by steering. With increasing kinetic energy more direct adsorption is favored. This may be caused by an increase in

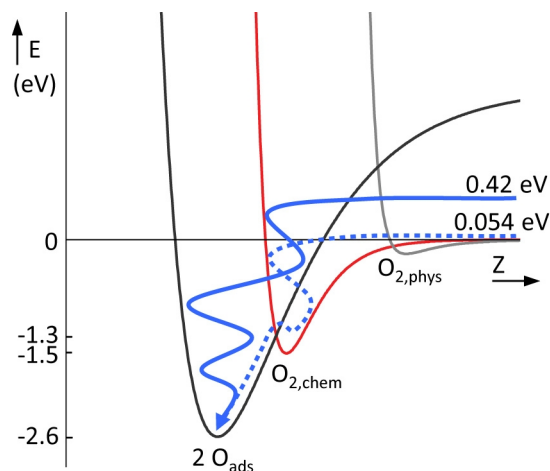


**Figure 3.7:** Schematic 1-D representation of the potential energy surface for  $O_2$  dissociation on Pd(100). Values of well depth and barrier from<sup>40,41</sup>. The dashed arrow shows the pathway for molecules with low  $E_i$ , the solid arrow for high  $E_i$ .

trajectories passing by the metastable molecular state at the fourfold hollow or an opening of modestly activated dissociation pathways at other locations in the unit cell. Although similar trends in reactivity are observed for various low-Miller indices of the same metal, the dynamics of dissociation appear distinctly different. The interpretation of our results is in part based on available cuts of high dimensionality PESs. However, theoretical studies have not quantitatively predicted reactivity for which we now present accurate data. It seems that theoretical dynamics studies will require proper treatment of phonon excitation in order to account for the observed trends. Furthermore, angle and coverage-dependence studies can verify our suggestions regarding the relevance of steering and sticking of  $O_2$  into a stabilized molecular state when coverage increases.

